Applied Materials Today 20 (2020) 100754

Contents lists available at ScienceDirect

Applied Materials Today

journal homepage: www.elsevier.com/locate/apmt

Continuous rheological description of highly filled polymer melts for material extrusion

Petr Filip [a], Berenika Hausnerova [b,c,*], Eva Hnatkova [b,c]

[a] Institute of Hydrodynamics, Czech Academy of Sciences, Pod Patankou 5, 166 12 Prague, Czech Republic
[b] Department of Production Engineering, Faculty of Technology, Tomas Bata University in Zlín, Vavreckova 275, 760 01 Zlín, Czech Republic;
[c] Centre of Polymer Systems, University Institute, Tomas Bata University in Zlín, Trida T. Bati 5678, 760 01 Zlín, Czech Republic

ARTICLE INFO

Article history:
Received 14 April 2020
Revised 11 June 2020
Accepted 1 July 2020

Keywords:
Material extrusion
Highly filled melts
Flow performance
True viscosity
Master curve

ABSTRACT

In additive manufacturing based on the material extrusion of filled polymer melts, a correct description of the rheological behaviour of the processed material is an important requirement. In case of highly filled feedstocks, complexities connected with a proper flow description are not only caused by the high packaging of powder particles (more than 50 vol.%) but also by the notable participation of polymer binder components in the quantification of shear viscosity. In this study, analytical expressions (master curves) of a true shear viscosity are developed to follow and continuously optimize the rheological dependence of the bulk feedstock on particular variables. A nickel-chromium-based compound (Inconel 718, content 59 vol.%) with thermoplastic binders of different molecular weight of polyethylene glycol was selected for the case study. The proposed master curves comprise simultaneously hitherto separately applied two corrections of an apparent shear viscosity: regarding the different capillary geometries with respect to entrance pressure and outlet extension, and determining an actual velocity profile based on shear rate distribution inside a feedstock. This approach eliminates the hitherto used non-Newtonian index, by means of which the logarithmic derivative was approximated. As the master curves depend exclusively on the shear rate and molecular weight of polyethylene glycol and do not involve any adjustable parameter, their application is straightforward. Their accuracy does not exceed experimental errors.

1. Introduction

The use of highly filled polymer compounds in additive manufacturing (AM) based on material extrusion is limited by the flow performance of the available feedstocks [1,2]. Its merging with powder injection moulding (PIM) [3] gives a possibility to adopt - besides powder characteristics - also the computer-aided engineering (CAE) approaches, which were originally developed for the PIM processes [4].

However, while the methodology of simulation of debinding and sintering steps is well established (e.g. in [5]), this has not been the case for part-forming step, where the rheological description of the used feedstocks faces instabilities and serious challenges [6–8], flow data fitting is provided based on the apparent values of shear stress and shear rates, and the discrete approximation of rheological parameters introduces errors in data fitting. Consequently, this has a direct impact (incorrect entry data) on reliability of simulations of the overall process.

Furthermore, in AM, the available rheological data [9–12] are rather scarce in the case of highly filled compounds compared to pure polymer materials [13–23]. Regardless of the detrimental issues, e.g., nozzle clogging caused by high viscosity and powder–binder separation, obtaining true values of shear viscosity subjects to two factors: 1) correctness of pressure induced in nozzles related to the flow inlet; 2) expansion of the feedstocks after leaving the nozzles, which is rather negligible due to combination high filler loadings and wall-slip [24].

Feedstock rheometry is not only complicated by high loadings of powder particles, but equally by presence of binder components and additives (dispersants, stabilizers, plasticizers, and intermolecular lubricants) [25]. Their impact on rheological characterization is even more substantial for AM than for PIM [1]. The problem is that the hitherto used rheological (constitutive) models are unable to include more than one component in the studied highly filled mixtures and only powder particles (partially geometrical shape) are considered. However, during simulation, it is necessary to optimize the contents of a binder.

This situation reflects the aim of this study. For metal powder processing, nickel–chromium-based powder particles (Inconel 718)

* Corresponding author at: Centre of Polymer Systems, University Institute, Tomas Bata University in Zlín, Trida T. Bati 5678, 760 01 Zlín, Czech Republic

https://doi.org/10.1016/j.apmt.2020.100754
2352-9407/

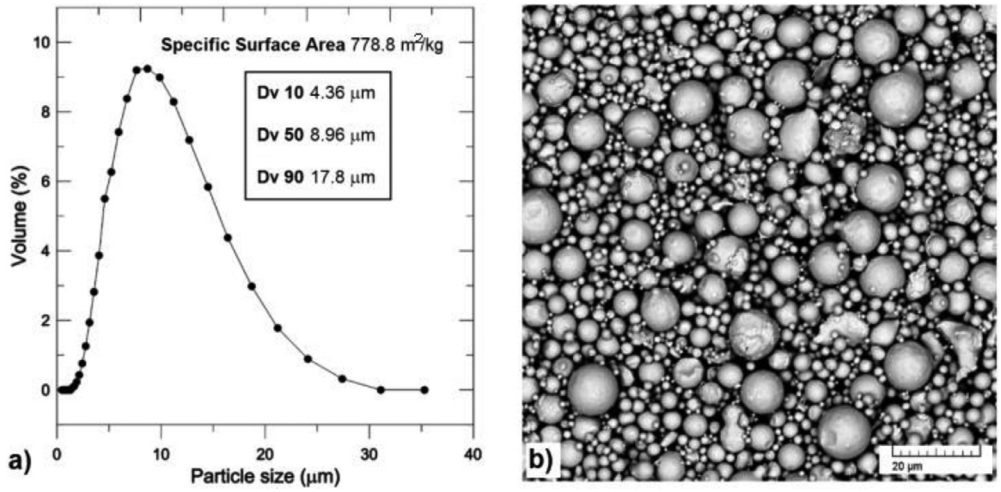

Fig. 1. Particle size distribution (a) and particle shape (b) of Inconel 718 powder.

were chosen and mixed with a binder comprising poly(ethylene glycol) (PEG), poly(methyl methacrylate), and stearic acid. While Claudel et al. [26] focused on the variation of particle size distribution of Inconel 718, we altered the molecular weight of PEG. A master curve depicting the apparent rheological behaviour of a feedstock with varying molecular weight of PEG is proposed, i.e., the corresponding constitutive model describing the apparent shear viscosity does not depend on any adjustable parameter, and the only parameter in this relation is represented by the molecular weight of PEG. This apparent master curve is used to significantly improve the accuracy of the resulting true shear viscosity of the feedstock described by the true master curve (again no fitting parameter), which includes the Bagley and Weissenberg–Rabinowitch corrections.

2. Experimental

2.1. Material

An analysed feedstock comprises 59 vol.% of nickel–chromium-based powder Inconel 718 (Sandvik Osprey Ltd, UK). In Fig. 1, the spherical shape of the powder particles is shown using a scanning electron microscope Vega II LMU (Tescan, Czech Republic). The particle size distribution (D_{10} = 4.36 μm, D_{50} = 8.96 μm, and D_{90} = 17.8 μm) was determined using a laser diffraction particle size analyser Mastersizer 3000 (Malvern, UK). The specific surface area is 779 m^2/kg.

The binder includes three components: 83 wt.% PEG (Sigma-Aldrich, USA), 15 wt.% poly(methyl methacrylate) particles (Scott Bader Co Ltd, UK; 0.1–0.2 μm; M_w ~ 10^6 g/mol), and 2 wt.% surfactant stearic acid (Prolabo Chemicals (VWR), USA). The stearic acid is widely used in feedstocks because of its positive contribution to high levels of packaging and flowability, substantially reducing the porosity of the final products [27].

In the present analysis, all the volumetric (59 and 41 vol.%) and weighted (83, 15, and 2 wt.%) percentages are fixed; the only altered parameter is the molecular weight of PEG, however, with a strong rheological impact. Five PEG materials with different molecular weights were evaluated using a high-performance liquid chromatography breeze system (Waters, USA), operated in the gel permeation chromatography (GPC) mode and coupled with an evaporative light scattering detector (ELSD, Waters 2424) set at a nebulizer temperature of 12°C, a drift tube temperature of 40°C, and an N_2 pressure of 0.4137 MPa. The separation was conducted using a Shodex Ohpak SB-806M HQ bed column ((300 × 8) mm, 13 μm particles) (Showa Denko K.K., Japan). The flow rate of the mobile phase (water) was 1.0 mL/min, and the injection volume was 10 μL. The GPC system was calibrated with narrow pullulan standards (ranging from 180 to 708,000 g/Varian). The polymer samples (~3 mg) were dissolved in 1 mL of deionized water and filtered prior to analysis. Data processing was done using the Empower software. Furthermore, the differential scanning calorimetry (DSC) measurement was applied to determine the melting ranges of individual PEG components (Pyris 6 DSC, Perkin Elmer, USA) under an atmosphere of argon with a gas flow of 20 mL/min at a heating rate of 10 K/min. The obtained results, including the notations of the PEG materials, are listed in Table 1.

Table 1
Weight-average molecular weight (M_w), number-average molecular weight (M_n), polydispersity index (PDI), and melting range of PEG

Sample notation	M_w (g/mol)	M_n (g/mol)	PDI (-)	Melting range (°C)
P11K	11,100	8,900	1.25	49–59
P15K	15,200	12,500	1.22	53–64
P20K	19,600	16,000	1.23	56–68
P27K	27,100	21,800	1.24	59–72
P37K	37,300	30,700	1.21	64–76

2.2. Rheological measurements

In contrast to rotational rheometers, the capillary ones can set pressure conditions that are almost similar to the conditions of industrial processes. However, the focus should be on the correct interpretation of the obtained data because of their use in simulations. Therefore, instead of using apparent shear rate/stress data to calculate the apparent shear viscosity as in the case of the comparison of feedstocks that include varying powder loads and/or binder compositions, true values are used. To obtain true values of shear viscosity, two types of corrections are used (derived for round capillaries):

1) Bagley correction – used to compensate different capillary geometries regarding entrance pressure and outlet extension
2) Weissenberg-Rabinowitch correction – used to compute the actual velocity (non-parabolic profile) and thus, shear rate distribution in a non-Newtonian fluid (feedstock).

Using a capillary rheometer, the apparent viscosity (η_a) is given by

$$\eta_a = \frac{\tau_a}{\dot{\gamma}_a}, \quad (1)$$

where τ_a is the apparent wall shear stress and $\dot{\gamma}_a$ is the apparent shear rate. These two quantities are expressed through physical and geometrical quantities by

$$\tau_a = \frac{\Delta pR}{2L}, \quad (2)$$

$$\dot{\gamma}_a = \frac{4\dot{Q}}{\pi R^3}, \quad (3)$$

where Δp is the measured pressure gradient (drop), R is the radius of a capillary die, L is the length of a die, and $\dot{Q}$ denotes the volumetric flow rate.

First, it is necessary to compensate pressure gradients (Bagley correction) regarding the corrections (Δp_{end}) at the entrance and exit sections of the capillary dies and to obtain the corrected (true) wall shear stress

$$\tau_c = \frac{(\Delta p - \Delta p_{end})R}{2L}. \quad (4)$$

Second, the transformation of a parabolic velocity profile inside the dies using the Weissenberg–Rabinowitch correction provides the corrected (true) shear rate

$$\dot{\gamma}_c(\tau_c) = \frac{4\dot{Q}}{\pi R^3}\left[\frac{1}{4}\left(3 + \frac{d\ ln\dot{\gamma}_a}{d\ ln\tau_c}\right)\right] \quad \left(= \dot{\gamma}_a\left[\frac{1}{4}\left(3 + \frac{d\ ln\dot{\gamma}_a}{d\ ln\tau_c}\right)\right]\right). \quad (5)$$

Third, the true shear viscosity can be determined finally

$$\eta_c = \frac{\tau_c}{\dot{\gamma}_c}. \quad (6)$$

The rheological measurements were carried out using a capillary rheometer Rheograph 50 (Goettfert, Germany). The dependency of viscosity on shear rate was analysed at 140°C using three round capillary dies (L/D ratios: 5/1, 10/1, and 20/1; $D = 1$ mm) and a "zero" die (L/D ratio: 0.2; $D = 1$ mm). All measurements were obtained in a controlled-rate mode (at a constant piston speed) at the shear rate range of 200–2500 s^{-1}. The obtained values are determined using the capillary die geometry, shear rate, and measured pressure drop.

3. Results and discussion

The analysis of the measured data is classified into three steps:

- Introduction of an apparent master curve to describe apparent shear viscosity covering sufficiently broad regions of the shear rates and molecular weights of PEG binder components; these are the only inputs in the master curve that does not include any adjustable (fitting) parameter
- Evaluation of entrance pressure and outlet extension (Bagley correction). This step introduces an explicit functional relation based on shear rates and molecular weights
- Application of the Weissenberg–Rabinowitch correction in its original form, i.e., using a logarithmic derivative. This is enabled by applying the explicit form of the apparent master curve and introducing a true master curve respecting the corrections. This approach eliminates hitherto used a non-Newtonian index (n), by means of which the logarithmic derivative is approximated.

3.1. Apparent master curve

The measurement of apparent viscosity was conducted at the discrete points of the apparent shear rate (200, 250, 500, 700, 1000, 1500, 2000, and 2500 s^{-1}). Five feedstocks differed only in terms of the molecular weights of the PEG binder components. The viscosity depends on the shear rate and the shear stress in a pseudoplastic manner, and as expected, it increases with the molecular weight of the PEG binder component.

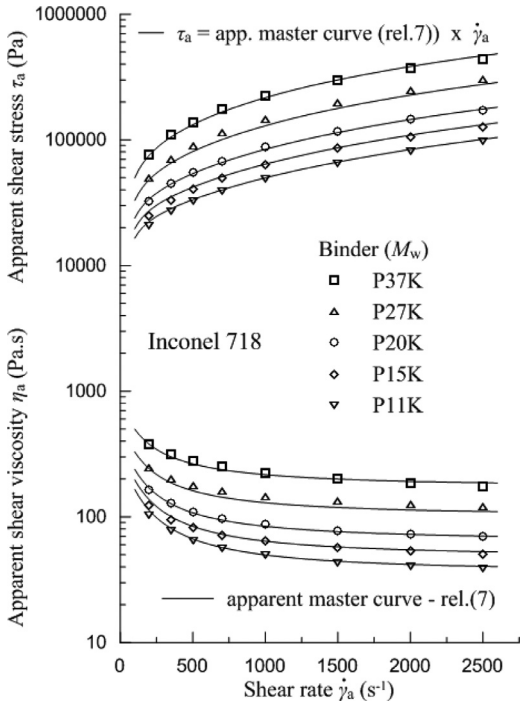

Fig. 2. Comparison between the experimental data and the apparent master curve prediction (rel .(7)).

Based on the analysis of the experimental data, the following relation for the apparent master curve describing apparent viscosity can be proposed

$$\eta_a = 23 + 0.105\ M_w{}^2 + 150000\ .\ (\dot{\gamma}_a + 105)^{(0.0067\ M_w - 1.4)}\ , \quad (7)$$

where $\dot{\gamma}_a$ (s^{-1}) is the apparent shear rate and M_w (kg/mol) is the molecular weight of the individual feedstocks. In deriving the functional form of Eq. (7) a relatively simple form of dependence of apparent viscosity on apparent shear rate was chosen: a 4-parameter power function $\eta_a = C_1 + C_2.(\dot{\gamma}_a + C_3)^{C_4}$, where consequently the parameters C_1 and C_4 were optimized as quadratic and linear functions of M_w, respectively. The comparison between the proposed apparent master curve and the experimental data is depicted in Fig. 2. Eq. (7) contains no adjustable parameters. Each individual curve in Fig. 2 corresponds to one chosen molecular weight (according to a binder composition). The upper curves express behaviour of apparent shear stresses and the lower ones behaviour of apparent shear viscosities in dependence on apparent shear rate. The mean deviation of apparent viscosity across all the measured points is 4.3 %. The functional form of Eq. (7) (and also below introduced equations) should not express its course only in pointwise approach but especially with emphasis to overall behaviour (first derivative: increase and decrease, second derivative: convexity and concavity). Such approximation then ensures a possibility to approximate behaviour of first derivative through the proposed functional forms.

3.2. Bagley correction

The Bagley correction evaluates the entrance pressure and outlet extension. For its analysis, three "non-zero" capillary dies (L/D ratios: 5/1, 10/1, and 20/1, $D = 1$ mm) and a "zero" die (L/D ratio 0.2, $D = 1$ mm) were used for P27K (Fig. 3). A similar linearity for individual shear rates was also observed for the remaining

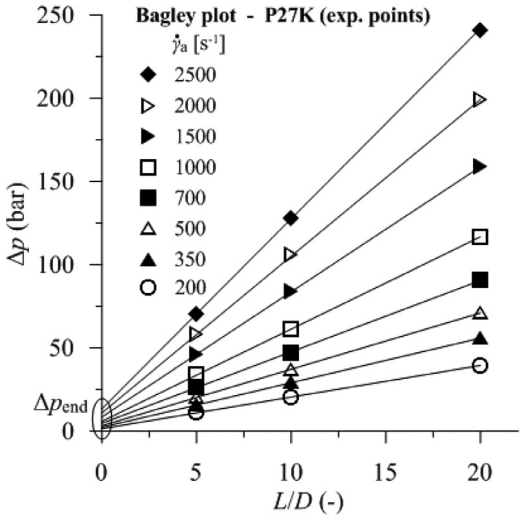

Fig. 3. Bagley plot of a material containing a PEG component with a molecular weight of 27.1 kg/mol.

Table 2
Deviation of the adjacent slopes in the Bagley plots.

$\dot{\gamma}_a$ (s^{-1})	Δ (angle) (°) P11K	P15K	P20K	P27K	P37K
200	0.5	1.6	0.4	0.1	0.3
350	0.3	0.8	0.4	0.6	0.3
500	0.9	1.1	0.1	0.2	0.1
700	0.2	0.5	0.2	0.5	0.0
1,000	0.7	0.8	0.2	0.0	0.5
1,500	0.8	0.5	0.2	0.1	0.1
2,000	0.2	0.4	0.1	0.1	0.0
2,500	0.3	0.5	0.2	0.1	0.1

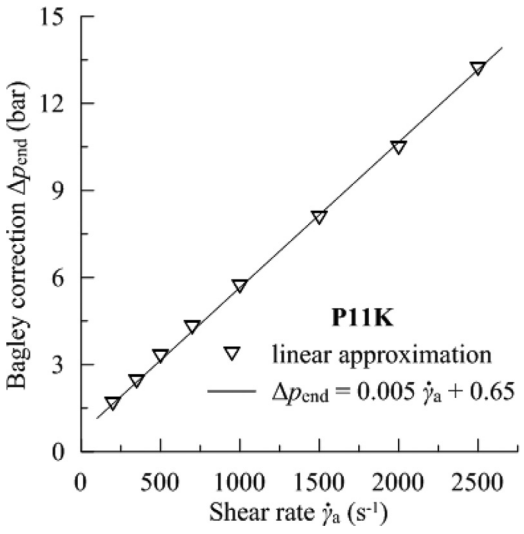

Fig. 4. Linear description of linearly approximated Bagley corrections for P11K.

molecular weights. The negligible deviation from linearity is listed in Table 2, where Δ (angle) is the difference between two consecutive segments connecting the following points: L/D = 20 and 10 and L/D = 10 and 5. This indicates the accuracy of the approximated Bagley correction (Δp_{end}) corresponding to L/D = 0.

Fig. 4 depicts the possibility of the linear description of the Bagley corrections Δp_{end} derived by a linear approximation at L/D = 0 for P11K. Based on the analysis of the Bagley corrections (Δp_{end}) for various molecular weights, the following relation can

Table 3
Values of the parameter K for the individual molecular weights.

Material	K = K(M_w)
P11K	1.00
P15K	0.87
P20K	0.42
P27K	1.02
P37K	0.72

be proposed

$$\Delta p_{end} \equiv \Delta p_{end}(\dot{\gamma}_a,\ M_w) = K(M_w)\ .(0.005\ \dot{\gamma}_a + 0.65), \tag{8}$$

where the parameter K = K(M_w) depending on the molecular weights is shown in Table 3. If we compare the values of the Bagley corrections (Δp_{end}) obtained using the linear interpolation (as indicated in Fig. 3) of all five materials with the approximated values generated by Eq. (2), the mean deviation of all 40 points attains 7 %, which is comparable with the experimental errors.

3.3. Weissenberg–Rabinowitch correction - true master curve

In Fig. 3, the slopes ($k(\dot{\gamma}_a,M_w)$) of the lines relating Δp and L/D are identical to the ones relating (Δp-Δp_{end}) with L/D for the same shear rates and molecular weights. Hence, the true corrected shear stress can be expressed as

$$\tau_c = \frac{(\Delta p - \Delta p_{end})R}{2L} = \frac{(\Delta p - \Delta p_{end})}{4L/D} = \frac{1}{4}\ k(\dot{\gamma}_a, M_w). \tag{9}$$

As indicated in Table 2, the optimized experimental values of slopes k exhibit completely negligible deviations from the experimental values. Therefore, if these 40 discrete points (5 molecular weights x 8 shear rates) are approximated by a sufficiently smooth surface plane (k above $\dot{\gamma}_a$ and M_w), then we have an approximated relation describing the course of corrected shear stress values. Based on the analysis of the experimental data, the following relation can be proposed

$$k(\dot{\gamma}_a, M_w) = 0.5 + A(M_w).\dot{\gamma}_a^{B(M_w)}, \tag{10}$$

where

$$A(M_w) = 0.0000046.M_w^{2.55}, \tag{11}$$

$$B(M_w) = 1.23 - 0.307.\log(M_w). \tag{12}$$

The deviation of this surface plane from the experimental data is depicted in Fig. 5, and its mean value is 2.5 %. Smoothness and negligible deviations ensure that the courses of the first and second derivatives with respect to the molecular weight and shear stress consider the convexity and concavity of the experimental surface plane as well. In other words, in the Weissenberg–Rabinowitch correction, a derivative can be realized with respect to $\dot{\gamma}_a$. After differentiating a logarithmic derivative in Eq. (5), we obtain

$$\dot{\gamma}_c(\tau_c) = \dot{\gamma}_a\left[\frac{1}{4}\left(3 + \frac{\tau_c}{\dot{\gamma}_a}.\left(\frac{d\tau_c}{d\dot{\gamma}_a}\right)^{-1}\right)\right] = \frac{3}{4}\ .\ \dot{\gamma}_a + \frac{1}{4}\ .\tau_c\ .\left(\frac{d\tau_c}{d\dot{\gamma}_a}\right)^{-1}, \tag{13}$$

where (according to Eqs. (9) and (10))

$$\frac{d\tau_c}{d\dot{\gamma}_a} = \frac{1}{4}\ .\ A(M_w)\ B(M_w).\dot{\gamma}_a^{B(M_w)-1}. \tag{14}$$

Then, an explicit relation for true (corrected) viscosity

$$\eta_c = \frac{\tau_c}{\dot{\gamma}_c} \tag{15}$$

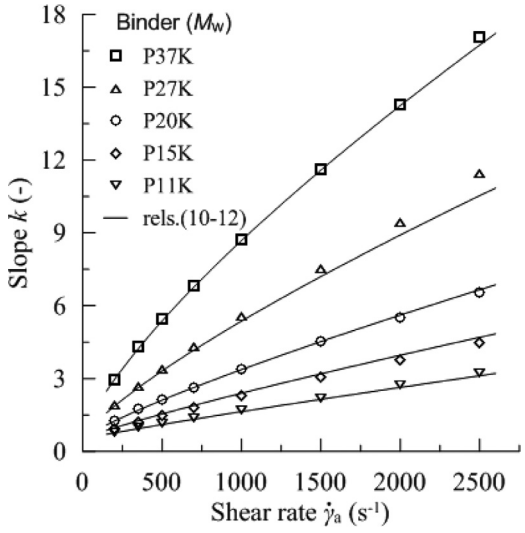

Fig. 5. Comparison of the experimental and predicted (rels. (10)–(12)) values of the slopes (k) in dependence on the molecular weights of PEG and shear rates.

is determined by the Eqs. (9)–(14). Comparing with Eq. (7), we can observe the discrepancies between the true (corrected) master curve and the apparent one. These are caused by respecting both Bagley and Weissenberg-Rabinowitch corrections which are quite often neglected without any substantiation. Consequently, this neglect resulting in incorrect entries to the following steps (debinding, sintering) significantly participates in worsen quality of the final products.

The proposed corrected master curve for corrected shear viscosity has the following advantages:

- A simple algebraic form comprising only additive and power terms (the unit of molecular weight should be kg/mol)
- No adjustable (fitting) parameter in the final relation
- Higher (continuous) coverage with very good accuracy related to $\dot{\gamma}_a$ (200–2500 s^{-1}) and M_w (11.1–37.3 kg/mol)

The nominal molecular weights of PEG supplied by the producers quite often differ from the real ones. Because of the continuous range of molecular weights, any value can be inserted in the final relation.

4. Conclusions

The optimization of feedstock compositions is difficult to implement if rheological behavior is only known for discrete values of the entry components. In simulation, it should comply with the continuous changes in the geometrical arrangement of material inlets and with the continuous adjustment of pressure gradients exerted to a feedstock. In our case, the proposed true (corrected) master curve provides an adequate solution as the shear viscosity can be determined for any molecular weight of PEG without considering any adjustable (fitting) parameter. The distinct advantage is that the true master-curve approximation does not exceed experimental errors in the whole intervals of the molecular weights of PEG and exerted shear rates.

Data aviability

The raw/processed data required to reproduce these findings cannot be shared at this time due to technical or time limitations.

Declaration of Competing Interests

The authors report no conflict of interest.

Declaration of Competing Interest

Authors have no conflict of interest.

CRediT authorship contribution statement

Petr Filip: Methodology, Data curation, Validation, Writing - original draft, Writing - review & editing, Funding acquisition. **Berenika Hausnerova:** Conceptualization, Supervision, Writing - original draft, Writing - review & editing, Funding acquisition. **Eva Hnatkova:** Resources, Investigation.

Acknowledgments

The author (P.F.) wishes to acknowledge the Czech Science Foundation for the financial support under Grant Project No. 17-26808S. The work was supported (B.H., E.H.) by the Ministry of Education, Youth and Sports of the Czech Republic—Program NPU I (LO1504).

References

[1] J.J. Fallon, S.H. McKnight, M.J. Bortner, Highly loaded fiber filled polymers for material extrusion: a review of current understanding, Addit. Manuf. 30 (2019) 100810 https://doi.org/10.1016/j.addma.2019.100810.
[2] J. Gonzalez-Gutierrez, S. Cano, S. Schuschnigg, C. Kukla, J. Sapkota, C. Holzer, Additive manufacturing of metallic and ceramic components by the material extrusion of highly-filled polymers: a review and future perspectives, Materials 11 (2018) 840–876 https://doi.org/10.3390/ma11050840.
[3] N. Williams, Threat or opportunity? The MIM industry as a partner, a target, and a market for metal AM, PIM Int. 12 (2018) 57–65 https://issuu.com/inovar-communications/docs/pim_vol_12_no_4_sp.
[4] T.G. Kang, S. Ahn, S.H. Chung, S.T. Chung, Y.S. Kwon, S.J. Park, R.M. German, Modeling and simulation of metal injection molding (MIM), in: D.F. Heaney (Ed.), Handbook of Metal Injection Molding, Second Edition, Woodhead Publishing, 2019, pp. 219–252. https://doi.org/10.1016/B978-0-08-102152-1.00013-1.
[5] M. Sahli, B. Mamen, H. Ou, J.-C. Gelin, T. Barrière, M. Assoul, Experimental analysis and numerical simulation of sintered micro-fluidic devices using powder hot embossing process, Int. J. Adv. Manuf. Techn. 99 (2018) 1141–1154 https://doi.org/10.1007/s00170-018-2509-5.
[6] T. Honek, B. Hausnerova, P. Saha, Temperature dependent flow instabilities of highly filled polymer compounds, Appl. Rheol. 12 (2002) 72–80 https://doi.org/10.3933/ApplRheol-12-72.
[7] B. Hausnerova, T. Sedlacek, P. Vltavska, Pressure-affected flow properties of powder injection moulding compounds, Powder Technol. 194 (2009) 192–196 https://doi.org/10.1016/j.powtec.2009.04.007.
[8] B. Hausnerova, T. Sedlacek, P. Filip, P. Saha, The effect of powder characteristics on pressure sensitivity of powder injection moulding compounds, Powder Technol. 206 (2011) 209–213 https://doi.org/10.1016/j.powtec.2010.08.065.
[9] K. Rane, L. Di Landro, M. Strano, Processability of SS316L powder - binder mixtures for vertical extrusion and deposition on table tests, Powder Technol. 345 (2019) 553–562 https://doi.org/10.1016/j.powtec.2019.01.010.
[10] C. Kukla, J. Gonzalez-Gutierrez, I. Duretek, S. Schuschnigg, C. Holzer, Effect of particle size on the properties of highly-filled polymers for fused filament fabrication, AIP Conf. Proc. 1914 (2017) 190006 https://doi.org/10.1063/1.5016795.
[11] Y. Thompson, J. Gonzalez-Gutierrez, C. Kukla, P. Felfer, Fused filament fabrication, debinding and sintering as a low cost additive manufacturing method of 316L stainless steel, Addit. Manuf. 30 (2019) 100861 https://doi.org/10.1016/j.addma.2019.100861.
[12] M. Schwentenwein, J. Homa, Additive manufacturing of dense alumina ceramics, Int. J. Appl. Ceram. Technol. 12 (2015) 1–7 https://doi.org/10.1111/ijac.12319.
[13] A.R. Torrado, C.M. Shemelya, J.D. English, Y. Lin, R.B. Wicker, D.A. Roberson, Characterizing the effect of additives to ABS on the mechanical property anisotropy of specimens fabricated by material extrusion 3D printing, Addit. Manuf. 6 (2015) 16–29 http://dx.doi.org/10.1016/j.addma.2015.02.001.
[14] L. Verbelen, S. Dadbakhsh, M. Van den Eynde, D. Strobbe, J.-P. Kruth, B. Goderis, P. Van Puyvelde, Analysis of the material properties involved in laser sintering of thermoplastic polyurethane, Addit. Manuf. 15 (2017) 12–19 http://dx.doi.org/10.1016/j.addma.2017.03.001.
[15] C. Ajinjeru, V. Kishore, P. Liu, J. Lindahl, A.A. Hassen, V. Kunc, B. Post, L. Love, C. Duty, Determination of melt processing conditions for high performance amorphous thermoplastics for large format additive manufacturing, Addit. Manuf. 21 (2018) 125–132 https://doi.org/10.1016/j.addma.2018.03.004.
[16] F. Liravi, M. Vlasea, Powder bed binder jetting additive manufacturing of silicone structures, Addit. Manuf. 21 (2018) 112–124 https://doi.org/10.1016/j.addma.2018.02.017.
[17] J. Stieghorst, T. Doll, Rheological behavior of PDMS silicone rubber for 3D printing of medical implants, Addit. Manuf. 24 (2018) 217–223 https://doi.org/10.1016/j.addma.2018.10.004.

[18] N.E. Zander, M. Gillan, R.H. Lambeth, Recycled polyethylene terephthalate as a new FFF feedstock material, Addit. Manuf. 21 (2018) 174–182 https://doi.org/10.1016/j.addma.2018.03.007.
[19] Z. Zhou, I. Salaoru, P. Morris, G.J. Gibbons, Additive manufacturing of heat-sensitive polymer melt using a pellet-fed material extrusion, Addit. Manuf. 24 (2018) 552–559 https://doi.org/10.1016/j.addma.2018.10.040.
[20] M.Q. Ansari, M.J. Bortner, D.G. Baird, Generation of polyphenylene sulfide reinforced with a thermotropic liquid crystalline polymer for application in fused filament fabrication, Addit. Manuf. 29 (2019) 100814 https://doi.org/10.1016/j.addma.2019.100814.
[21] S.B. Balani, F. Chabert, V. Nassiet, A. Cantarel, Influence of printing parameters on the stability of deposited beads in fused filament fabrication of poly(lactic) acid, Addit. Manuf. 25 (2019) 112–121 https://doi.org/10.1016/j.addma.2018.10.012.
[22] E.-J. Courtial, C. Perrinet, A. Colly, D. Mariot, J.-M. Frances, R. Fulchiron, C. Marquette, Silicone rheological behavior modification for 3D printing: evaluation of yield stress impact on printed object properties, Addit. Manuf. 28 (2019) 50–57 https://doi.org/10.1016/j.addma.2019.04.006.
[23] J. Clayton, D. Millington-Smith, B. Armstrong, The application of powder rheology in additive manufacturing, JOM 67 (2015) 544–548 https://doi.org/10.1007/s11837-015-1293-z.
[24] B.K. Aral, D.M. Kalyon, Viscoelastic material functions of noncolloidal suspensions with spherical particles, J. Rheol. 41 (1997) 599–620 https://doi.org/10.1122/1.550841.
[25] B. Hausnerova, V. Kasparkova, E. Hnatkova, Effect of backbone binders on rheological performance of ceramic injection molding feedstocks, Polym. Eng. Sci. 57 (2017) 739–745 https://doi.org/10.1002/pen.24621.
[26] D. Claudel, M. Sahli, T. Barriere, J.C. Gelin, Influence of particle-size distribution and temperature on the rheological properties of highly concentrated Inconel feedstock alloy 718, Powder Technol. 322 (2017) 273–289 https://doi.org/10.1016/j.powtec.2017.08.049.
[27] M. Aslam, F. Ahmad, P.S.M.B.M. Yusoff, K. Altaf, M.A. Omar, R.M. German, Powder injection molding of biocompatible stainless steel biodevices, Powder Technol. 295 (2016) 84–95 https://doi.org/10.1016/j.powtec.2016.03.039.